

# Studies of structural, magnetic, electrical and photoconducting properties of $\text{Bi}_{1-x}\text{Ca}_x\text{MnO}_3$ epitaxial thin films.

S. Chaudhuri and R. C. Budhani\*

*Department of Physics*

*Indian Institute of Technology Kanpur*

*Kanpur - 208016, India*

(Dated: September 27, 2018)

## Abstract

The dynamics of the charge ordered (CO) state under non-equilibrium conditions created by strong dc-electric field ( $\leq 10^6$  V/cm) and photo-illumination with short ( $\approx 6$  ns) laser pulses is investigated in  $\text{Bi}_{1-x}\text{Ca}_x\text{MnO}_3$  ( $x > 0.5$ ) epitaxial films. A pulsed laser deposition method was used to synthesize films on (100)  $\text{LaAlO}_3$  (LAO) and (100)  $\text{SrTiO}_3$  (STO) substrates. The crystallographic structure, temperature dependence of electrical resistivity and magnetization of the samples of different composition prepared under different oxygen partial pressure ( $p\text{O}_2$ ) and deposition temperature ( $T_D$ ) are studied. For the  $x = 0.6$  sample grown on LAO, a clear signature of charge ordering at  $\approx 275$  K is seen in the magnetization and at  $\approx 260$  K in the resistivity data. The same sample grown on STO revealed a complex behavior, which entails charge ordering at  $\approx 300$  K, a Néel order at  $\approx 150$  K and finally a weak ferromagnetic phase below 50 K. A strong correlation between charge ordering temperature ( $T_{CO}$ ) and the c-axis lattice parameter ( $c$ ) of the type ( $dT_{CO}/dc \approx -350$  K/Å) emerges from measurements on films deposited under different growth conditions. Since the out of plane lattice parameter ( $c$ ) increases with in plane compressive strain, this effect directly shows a compressive strain induced suppression of the  $T_{CO}$ . The current (I)-voltage (V) characteristics of the samples at  $T < T_{CO}$  show hysteresis due to a compound effect of Joule heating and collapse of the CO state. Transient changes in conductivity of lifetime ranging from nano to microseconds are seen at  $T < T_{CO}$  on illumination with pulsed UV (355 nm) radiation. These observations are explained on the basis of the topological and electronic changes in the charge ordered phase.

PACS numbers: 75.25.+z, 78.20.Ls, 42.65.Ky, 75.30.Et

## I. INTRODUCTION

The manganite  $\text{Bi}_{1-x}\text{Ca}_x\text{MnO}_3$  (BCMO) is a fairly well studied system in the bulk ceramic and single crystal forms.<sup>1,2,3,4,5,6,7</sup> BCMO is known to exhibit Charge Ordering (CO) over a much broader range of hole doping than its isostructural counterpart,  $\text{La}_{1-x}\text{Ca}_x\text{MnO}_3$ . But the key property that makes BCMO stand out, atleast from the technological view point, is its behavior upon photoillumination. Manganites are known to exhibit the coexistence of a charge ordered insulating (COI) and charge delocalized ferromagnetic metallic (CDFM) phases under the non-equilibrium conditions created by photoillumination, whereby regions exposed to the photon field undergo a transition from the initially insulating to a metallic state leaving the unexposed regions unaffected.<sup>8,9,10,11,12,13,14,15,16,17,18</sup> Owing to the difference in their electrical conductivity, the exposed and the unexposed regions have different refractive indices. This feature, along with the localized nature of the photoinduced insulator-to-metal transition (IMT), can be exploited for the creation of photonic bandgap structures using holographic techniques.<sup>6</sup> But in most of the manganites this effect is transient as the pressure on the conducting phase from the surrounding insulating matrix forces it back to its insulating state, and makes the practical realization of manganites as photonic bandgap crystals a challenging issue. However, unlike the other charge ordered manganites, BCMO has been found to exhibit a persistent change in properties on photoillumination.<sup>6</sup> Owing to this extraordinary property, BCMO is a promising candidate for photonic crystals. BCMO is well studied in its bulk form, Woo *et al.*<sup>3</sup> have performed resistivity, magnetization, X-ray absorption as well as X-ray diffraction measurements to correlate the structural, magnetic and transport properties of BCMO. They reported the charge ordering temperature  $T_{CO}$  for  $x = 0.4, 0.6,$  and  $0.8$  to be 315 K, 330 K, and 190 K and the Néel temperature  $T_N$  for  $x = 0.4,$  and  $0.6,$  to be 150 K, and 125 K respectively, and point out the importance of Mn-O bond distortion in stabilizing the CO phase. Bokov *et al.*<sup>1</sup> have given a detailed account of the structural properties along with electrical transport and magnetic properties for  $0.2 \leq x \leq 1$ . Podzorov *et al.*<sup>5</sup> found that the transformation to the charge ordered state to be martensitic in character. This non-diffusive transformation by its very nature, leads to long-range deformation of the crystal lattice and results in accommodation strain at the charge ordered domain boundaries. Since, the martensitic strain is different from the substrate induced lattice deformation, a compound effect of these two strains in thin film

samples can either enhance or suppress the properties seen in bulk single crystals. These issues make studies on epitaxial thin films of BCMO important. So far only a limited study of photoconductivity in thin films of  $\text{Bi}_{1-x}\text{Ca}_x\text{MnO}_3$  on illumination with Ar-ion CW laser of mixed wavelength has been reported.<sup>19</sup>

This paper presents a detailed investigation of the growth conditions, structure, electrical transport, magnetic ordering and transient photoconductivity on pulsed laser illumination on three different compositions of  $\text{Bi}_{1-x}\text{Ca}_x\text{MnO}_3$  films in the overdoped regime. Studies on thin films are desirable as any conceivable practical application of photoinduced effects and related metal-insulator transition require the material in a thin film form. Furthermore, an epitaxial film supported on a substrate is likely to have fundamentally different properties due to quantum size effects and substrate related changes in stress and growth morphology.<sup>20,21,22</sup> With this in mind, we have prepared epitaxial thin films of  $\text{Bi}_{1-x}\text{Ca}_x\text{MnO}_3$  with  $x = 0.6, 0.67$  and  $0.76$  on STO (100) and LAO (100). The deposition temperature and the oxygen partial pressure were optimized to obtain films of good crystalline quality and the variation of the lattice parameters as a function of these growth parameters were studied by X-ray diffraction. Electrical resistivity and magnetization measurements on the  $x = 0.6$  sample reveal clear signatures of charge ordering at  $\approx 260$  K and  $\approx 275$  K respectively. The electric field dependence of charge transport in the CO - state is highly non-linear and shows history effects, whose origin is both thermal and electronic. The photoresponse measurements on  $x = 0.6$  sample exhibit a transient conducting state which can be attributed to the melting of the charge ordered state followed by freezing to the original insulating state over time scale of several microseconds. The measurement of current transport as well as photoeffects reveal a robust CO - state in BCMO.

## II. EXPERIMENTAL

Thin films of thickness  $\approx 2000$  Å of  $\text{Bi}_{1-x}\text{Ca}_x\text{MnO}_3$  with  $x = 0.6, 0.67$  and  $0.76$  were grown at the rate of  $\approx 1$  Å/sec on (100) oriented single crystals of  $\text{LaAlO}_3$  (rhombohedral with  $a = 3.788$  Å) and  $\text{SrTiO}_3$  (cubic with  $a = 3.905$  Å) using pulsed laser deposition (PLD) technique. A KrF excimer laser operated at 10 Hz with an areal energy density of  $2$  J/cm<sup>2</sup>/pulse on the surface of a stoichiometric sintered target of BCMO was used for ablation. The film growth conditions were optimized by varying the deposition temperature ( $T_D$ ) and oxygen

partial pressure ( $pO_2$ ) to realize a sharp step in electrical resistivity at  $T_{CO}$ . The films with the most prominent signature of charge ordering were obtained for  $T_D$  and  $pO_2$  of  $\approx 800$  °C and 350 mTorr respectively by ablation of the target of  $x = 0.6$ . The crystallographic structure and the surface roughness of the films were probed with X-ray  $\Theta-2\Theta$  diffraction and atomic force microscopy (AFM) techniques respectively. The AFM measurements revealed a smooth surface of roughness  $< 25$  Å. All magnetization measurements were carried out using a SQUID magnetometer [Quantum Design MPMS XL5]. Measurements of electrical resistivity, current-voltage characteristics (I-V) and photoinduced changes in resistivity were carried out on 1 mm wide strips of the film on which silver pads were deposited through shadow mask for connecting current and voltage leads. We have made bridges of length  $\geq 1$   $\mu$ m by using silica fibers as masks. The standard four probe technique was used to measure the electrical resistivity. Short pulses ( $\approx 6$  ns) of the third harmonic frequency ( $\lambda = 355$  nm) of an Nd:YAG laser were used for photoexcitation experiments. Changes in the voltage drop across the sample on photoillumination were captured using a fast digital oscilloscope (Tektronix TDS-380) with a time resolution of 0.5 ns.

### III. RESULTS AND DISCUSSION

#### A. Structural characterization

In Fig. 1 we show the X-ray diffraction profiles of the samples with  $x = 0.6$  grown at different  $pO_2$  but at the same  $T_D$  of 750 °C. The diffractograms are dominated by the strong (002) reflection of  $LaAlO_3$  next to which a small shoulder corresponding to (002) reflection of the BCMO appears. This feature has been marked by an arrow in the figure. The inset of Fig. 1 shows the variation of the out-of-plane lattice parameter ( $c$ ) as the  $pO_2$  is changed. For the sample deposited at  $pO_2$  of 350 mTorr, the  $c$  is  $\approx 3.81$  Å, in close agreement with the bulk value  $\approx 3.82$  Å calculated by Bokov *et al.*<sup>1</sup> X-ray diffraction measurements on samples deposited on LAO at  $pO_2 = 350$  mTorr and different  $T_D$  reveal that the crystalline quality of the thin films degrades on lowering the  $T_D$  below  $\approx 700$  °C. The X-ray diffraction patterns for samples of different composition grown at  $T_D = 750$  °C and  $pO_2 = 350$  mTorr are shown in Fig 2. The  $c$ -axis lattice parameter is found to decrease with increasing calcium content, as observed in bulk samples.<sup>1</sup> This compositional variation of the lattice parameter is due to

the fact that the end members  $\text{BiMnO}_3$  and  $\text{CaMnO}_3$  have monoclinic (with  $a = c = 3.932$  Å,  $b = 3.989$  Å) and cubic ( $a = 3.725$  Å) structures respectively. For the sake of comparison, in Fig. 3 we show the diffraction pattern of the sample grown on STO at  $p\text{O}_2$  of 350 mTorr and  $T_D$  of 750 °C. The out-of-plane lattice parameter  $c$  is 3.75 Å in this case, which is less by  $\approx 2\%$  as compared to the film deposited on LAO under similar conditions. Clearly the growth of BCMO films on STO puts a tensile strain on the a-b plane of the BCMO, and in order to maintain the unit cell volume the c-axis undergoes a contraction.

## B. Magnetic ordering

Figure 4 shows the temperature dependence of magnetization (M) measured at 0.5 tesla in-plane field in field-cooled (FC) and zero field-cooled (ZFC) modes for the  $x = 0.6$  sample grown at 750 °C and  $p\text{O}_2$  of 350 mTorr. The maxima in the magnetization at  $\approx 275$  K is similar to the observations of Woo *et al.*<sup>3</sup> on bulk crystals of BCMO. We identify the peak in magnetization to  $T_{CO}$ . However, this temperature is significantly lower than the  $T_{CO}$  of bulk samples ( $\approx 330$  K).<sup>3</sup> Also, unlike the case of bulk samples, the magnetization of these thin films below  $T_{CO}$  does not show a clear signature of antiferromagnetic ordering. The inset of Fig. 4 shows the M-H curve of the same sample measured at 200 K. The dependence of magnetization on field consists of a linear and a non-linear component. The spontaneous magnetization deduced by extrapolation of the linear component to  $H = 0$  comes out to be  $\approx 0.1 \mu_B$  per Mn ion. Since in a fully aligned ferromagnetic state this moment should be  $3.4 \mu_B$  per Mn ion, the small value of spontaneous moment suggests the presence of ferromagnetic correlation at  $T < T_{CO}$ . In Fig. 5 the temperature dependence of magnetization (M-T) of the  $x = 0.6$  sample deposited at  $T_D = 750$  °C and  $p\text{O}_2 = 170$  mTorr is shown. A comparison of these data with Fig. 4 shows a clear shift of the peak in magnetization to lower temperatures ( $\approx 260$  K) when the  $\text{O}_2$  partial pressure is reduced. This feature in M-T curve becomes a mere hump centered at  $\approx 250$  K when the  $\text{O}_2$  partial pressure is lowered further to 70 mTorr (see Fig. 6). An interesting feature of the magnetization curves of samples deposited at reduced  $\text{O}_2$  partial pressures is the splitting of the ZFC and the FC branches of the M-T curve at lower temperatures. This observation suggests the existence of ferromagnetically ordered clusters whose magnetization is blocked below a critical temperature. In the inset of Fig. 6 we show the magnetization data for the  $x = 0.6$  sample deposited at 750 °C and

650 mTorr. A cusp in the magnetization at  $\approx 285$  K marks the  $T_{CO}$ . This is followed by a weak signature of  $T_N$  around 110 K. The cusp-like feature in magnetization, which has been assigned to  $T_{CO}$  in single crystal and bulk samples, is pronounced in films deposited at high  $pO_2$  suggests a direct correlation between oxygen concentration in the films and charge ordering. In Fig. 7, the result of M vs T measurement at 0.5 tesla in-plane field on a  $x = 0.6$  sample grown at  $T_D = 750^\circ\text{C}$  and 350 mTorr  $pO_2$  on (001) STO substrate is shown. Two broad but distinct maxima in the M vs T plot observed at  $\approx 300$  K and  $\approx 120$  K can be identified with  $T_{CO}$  and  $T_N$  following the results on bulk samples where these temperatures are 330 K and 125 K respectively.<sup>3</sup> A marked difference in the ZFC and FC curves is also observed below  $\approx 50$  K. From the XRD analysis it was found that  $c$  for the  $x = 0.6$  sample grown at  $750^\circ\text{C}$  on LAO at 650 mTorr and STO at 350 mTorr were found to be  $3.76 \text{ \AA}$  and  $3.75 \text{ \AA}$  respectively. The similarity of the magnetization curve and the closeness of the  $c$  value seen here indicates that the lattice strain plays a decisive role in determining the sample properties. The inset of Fig. 7 shows M-H measurements at 10 K and 200 K. The magnetic moment at both these temperatures is non-linear at lower values of the applied field. The non-linear component saturates to values which correspond to  $\approx 0.11 \mu_B$  and  $\approx 0.17 \mu_B$  moment per Mn ion at 200 K and 10 K respectively. Consistent with the behavior of ZFC and FC magnetization at  $T \approx 50$  K, the M-H curve at 10 K also show a hysteresis. The extremely small value of the non-linear magnetization is consistent with measurements on bulk samples which shows AF ordering in this temperature range. The presence of hysteresis suggests that the bulk anti-ferromagnetic state also has a ferromagnetic component. This kind of spin clustering and glassy behavior has been observed in bulk samples with  $x = 0.875$ .<sup>7</sup> A comparison of the  $c$ -axis lattice parameter ( $c$ ) and  $T_{CO}$  deduced from XRD and magnetization measurements respectively reveal an inverse correlation between  $c$  and  $T_{CO}$ . This is shown in Fig. 8 for the  $x = 0.6$  films deposited at  $750^\circ\text{C}$  on LAO at different  $pO_2$  and on STO at 350 mTorr. The variation of  $T_{CO}$  with  $c$  is linear with a slope of  $\approx -350 \text{ K/\AA}$ . Since the out of plane lattice parameter increases with inplane compressive strain, this observation directly shows a compressive strain induced suppression of the charge ordering temperature.

### C. Linear and non-linear electrical transport

In Fig. 9 we show the temperature dependence of the electrical resistivity ( $\rho(T)$ ) for the  $x = 0.6$  samples deposited at different temperatures but at the same  $pO_2$  of 350 mTorr. The  $\rho(T)$  plots of samples deposited at  $T_D \approx 750$  °C show a rapid increase in the resistivity below a critical temperature  $T^*$  ( $\approx 260$  K). The presence of this feature is enhanced if we plot the differential resistivity ( $d\rho/dT$ ) vs  $T$  as shown in the inset for the sample deposited at  $T_D \approx 750$  °C. Since the magnetization of these samples (Fig. 4) also goes through a peak in the vicinity of this temperature, we identify it with the charge ordering temperature  $T_{CO}$ . The sudden rise in resistivity below the  $T_{CO}$  is due to the suppression of carrier hopping which is responsible for charge transport in the charge disordered paramagnetic state existing at  $T > T_{CO}$ . The charge ordered state in this system is quite robust as external field of strength  $\leq 5$  tesla does not produce any change in the resistivity. In Fig. 10 we show the variation of resistivity of the samples with different composition but grown at the same  $T_D$  ( $= 750$  °C) and  $pO_2$  (350 mTorr). A distinct step in the resistivity that corresponds to  $T_{CO}$  is seen only for the  $x = 0.6$  sample. This observation is consistent with the data on bulk samples<sup>3</sup>, where the sharpness of the step in  $\rho(T)$  at  $T_{CO}$  diminishes as the Ca concentration is increased. In Fig. 11 the temperature dependence of the resistivity of the  $x = 0.6$  sample deposited at  $T_D = 750$  °C but at different  $pO_2$  is shown. Good quality films showing a well defined step at  $T_{CO}$ , are found to grow in the  $pO_2$  regime of 170 to 350 mTorr. From these studies we can conclude that best conditions for the growth of charge ordered BCMO films correspond to  $T_D = 750$  °C - 800 °C and  $pO_2 \approx 170 - 350$  mTorr. In Fig. 12 we show the temperature dependence of resistivity of the  $x = 0.6$  sample grown on STO at 750°C and 350 mTorr  $pO_2$ . In this sample the step in the resistivity at  $T_{CO}$  is not very pronounced as compared to the sample grown on LAO. The inset shows the variation of the differential resistivity as a function of temperature. The kink in this graph at  $\approx 310$  K corresponds to the  $T_{CO}$ , which is close to the value obtained from the magnetization measurements on this sample. The in-plane resistivity of the film on STO is approximately one order magnitude larger than that of the sample grown on LAO. This observation can be understood on the basis of increased tensile strain which reduces the Mn-O-Mn orbital overlap in the plane of the film thereby favoring electron localization.

We have analyzed the temperature dependence of electrical resistivity of the  $x = 0.6$

samples at  $T < T_{CO}$  in some detail. A thermally activated transport due to excitation of carriers across a charge order gap should lead to a resistivity of the form  $\rho = \rho_0 \exp[\Delta E/K_B T]$ . A plot of  $\ln \rho$  vs  $1/T$  (not shown) showing a continuously changing slope of this curve as temperature is lowered below  $T_{CO}$  is indicative of a temperature dependent activation energy ( $\Delta E(T)$ ). For the sample deposited at 750 °C for example, the activation energy changes from 0.2 eV to 0.1 eV as the temperature is lowered from  $T_1$  (= 225 K) to  $T_2$  (= 150 K). At  $T < T_2$ , the activation energy remains nearly constant. The simplest scenario that can account for such a dependence of  $\Delta E$  is presented by Mott variable range hopping (VRH) process.<sup>23</sup> The VRH transport in a Fermi glass<sup>23</sup> leads to a resistivity of the type  $\rho(T) = \rho_0 \exp[(T_0/T)^{1/4}]$ , where  $\rho_0$  is the preexponential factor and  $T_0$  is related to the density of localized states at the Fermi energy  $N(E_F)$  through the relation  $K_B T_0 = 18\alpha^3/N(E_F)$ . In Fig. 13 we show plots of  $\ln(\rho)$  vs  $T^{1/4}$ . The VRH formalism was found to be in better agreement with the behavior of  $\rho(T)$  at  $T < T_{CO}$ . The slopes of these curves yield  $K_B T_0$  of 11 KeV, 16 KeV and 14 KeV for the sample deposited at 700, 750 and 800 °C respectively. The value of  $K_B T_0$  for the sample grown on STO was found to be 19 KeV. A calculation of the localization length  $a = (1/\alpha)$  from the  $K_B T_0$  requires a knowledge of the  $N(E_F)$ , which can be estimated from the measurement of the electronic specific heat or Pauli spin susceptibility. While specific heat has been measured for less-than-half-filled manganites<sup>24,25,26</sup>, such studies are lacking in the case of BCMO. The electronic susceptibility is also overwhelmed by the contribution from the localized  $t_{2g}$  spins at the Mn sites. In view of these limitations, the observation of VRH only signifies the presence of disorder in the medium.

It is experimentally well established that the charge ordered manganites with less-than-half-filling (LTHF) show fascinating effects of electric field on charge transport.<sup>27,28,29</sup> In order to see if similar effects also exists in this more-than-half-filled (MTHF) material, we have carried out the measurement of current-voltage characteristics of the best film of  $x = 0.6$ . All measurements were done in the constant voltage mode. The variation of the circuit current ( $I$ ) as a function of applied circuit voltage ( $V$ ) was measured at different temperatures by calculating the drop across a 1 k $\Omega$  metal film resistor connected in series with the sample. Holding the temperature constant, the applied voltage ( $V$ ) was swept up to a maximum value and then swept down at the same rate. In Fig. 14 (a) results of I-V measurements at different temperatures are shown. When the applied voltage across the



sample reaches a threshold value  $V^*$ , the sample makes a transition from the insulating state to a low resistive state as seen from the sudden jump in the current  $I$ . On further increasing the applied voltage, the current in the circuit is limited by the standard resistor in series with the sample. The sample switches back to its insulating state on decreasing the  $V$  but at a value much lower than the  $V^*$ . This results in a hysteretic I-V curve. Such hysteretic behavior has been seen abundantly in less-than-half-filled manganites.<sup>27,28,30</sup> However, unlike the case of LTHF manganites where the hysteretic response disappears on measuring the I-V again at the same temperature, here repeated measurements at the same temperature produce a hysteretic response. The lifetime of the current driven conducting state is only a few seconds after switching off the electric field. This observation suggests that the metallic state is perhaps induced by sample heating. We have repeated these measurements on several samples of different bridge dimensions and the switching is observed in all cases. The switching voltage depends upon the bridge dimension, for smaller length of the bridge, the current switching occurs at lower voltages. In Fig. 14 (b) the circuit current ( $I$ ) is plotted as a function of the voltage ( $V$ ) across the sample at 120 K. The bridge width was 50  $\mu\text{m}$ . These measurements were done simultaneously with the measurements shown in Fig. 14(a). Similar behavior of I-V curves has been observed in epitaxial thin films of  $\text{Sm}_{0.5}\text{Sr}_{0.5}\text{MnO}_3$  by Oshima *et al.*<sup>31</sup> The negative differential resistance exhibited by the sample in the electric field induced low resistive state strongly suggests that the current path is filamentary in nature.<sup>18,28</sup> Similar kind of switching behavior was also seen for the sample grown on STO. In order to address this issue in detail, the I-V measurements were performed by varying the width ( $t_w$ ) of the voltage pulse and the time delay ( $t_d$ ) between two successive pulses. It was found that as the time interval between pulses is reduced ( $t_d \approx 1$  sec) the current switching occurs gradually. It was also observed that when this interval was increased ( $t_d \approx 12$  sec), there was no current switching at all, even for the highest  $V$ , as shown in Fig. 15. This observation suggests that the current-switching phenomenon in this MTHF manganite is primarily thermal in nature. However, if the measurements are repeated at a particular temperature keeping  $t_d$  same for all the scans and by making sure that sample reaches thermal equilibrium after each scan, it is found that for later scans current switching occurs at a lower value of the voltage ( $V^*$ ) as seen in Fig. 16. However, the  $V^*$  does not keep decreasing with the increasing number of scans, but reaches a constant value  $V_C^*$  after few scans, typically five. Here it needs to be emphasized that if the current

switching was purely a heating effect, the same nature of the I-V curves would appear for all scans, until and unless enough thermalization time is not given, which is not the case here. Interestingly, the virgin behavior of I-V curve at a particular temperature  $T < T_{CO}$  is recovered ( $V^* > V_C^*$ ) after cycling the sample to  $T > T_{CO}$ . From the data of Fig. 14, 15, and 16 it can be argued that the bias dependence of the current transport in these films is a compound effect of simple heating, which is reversible, and a fractional permanent change in the topology of the CO state which creates patches of conducting regions. These conducting domains appear to grow in size during successive I-V cycles till saturation. This causes the circuit voltage, at the point of switching to reach the constant value ( $V_C^*$ ) after a few scans. It is to be noted that while measuring I-V characteristics at different temperatures the lowest temperature measurement was done first, and repeated scans were made to establish the constant voltage ( $V_C^*$ ) and then only the temperature was increased. Charge ordering becomes more and more robust as the temperature is decreased below  $T_{CO}$ . This causes the  $V_C^*$  to increase with decreasing temperature as shown in the inset of Fig. 16. It should be recalled that in less-than-half-filled manganites ( $x < 0.5$ ) of marginal bandwidth<sup>32,33,34</sup>, the energy difference between the CDFM and CO states is small, and the system can switch from CO to CDFM states on application of small perturbations. For more-than-half-filled manganites ( $x > 0.5$ ) such as the  $\text{Bi}_{0.4}\text{Ca}_{0.6}\text{MnO}_3$  in particular, there is no evidence for the formation of a CDFM state. The observed response here is a mixture of thermal and electronic effects.

#### D. Photoresponse measurements

We have also studied the stability of the charge ordered state under illumination with 355 nm pulsed radiation. These measurements were done in isothermal mode by biasing the circuit at a fixed voltage  $V \leq V_C^*$ , where  $V_C^*$  is the circuit voltage at which the circuit current shows the distinct step. The oscilloscope was connected directly across the sample to record the conductivity profile, in terms of the voltage drop, in real time. These measurements were done at temperatures where the sample resistance was orders of magnitude less than the input impedance of the scope. Fig. 17 shows the transient conducting state (TCS) induced by the 6 ns laser pulse at 120 K where the sample is initially insulating [ $V < V_C^*$ ]. The photon flux was  $\approx 10^{15}$  photon/mm<sup>2</sup> which corresponds to an energy density of 0.16 J/cm<sup>2</sup>.

The profile has a leading edge that follows the pulse shape. Here the sample resistance drops precipitously. This is followed by a tailing effect where the sample recovers its original insulating state. This recovery can be modeled by a bounded exponential growth function of the form  $V(t) = V_0 + V_1(1 - e^{-t/\tau})$ . The value of  $\tau$ , which signifies the time constant was found to be  $\approx 2.4 \mu\text{s}$ . In Fig. 18 we show the dependence of the photoresponse on incident power for a given bias voltage. A power of 90% in the figure corresponds to energy density of  $0.16 \text{ J/cm}^2$ . Two features of these data are noteworthy. First, the response has a damped oscillatory behavior over short time scale of the recovery process ( $\approx 2 \mu\text{s}$ ). A similar behavior has also been observed by Miyano *et al.*<sup>8</sup> in the case of  $\text{Pr}_{0.7}\text{Ca}_{0.3}\text{MnO}_3$  crystals. This is an effect of the sudden voltage drop across the sample caused by the large photocurrent. Secondly the photoresponse is non-linear in power as shown in the inset of Fig. 18. The threshold power required for an observable change is  $\approx 40\%$ . The fundamental difference between the photoresponse of BCMO as studied here and those of less-than-half-filled charge ordered manganites such as  $\text{Pr}_{0.7}\text{Ca}_{0.3}\text{MnO}_3$ <sup>10</sup> and  $\text{Pr}_{1-X}(\text{Ca}_Y\text{Sr}_{1-Y})_X\text{MnO}_3$ <sup>11</sup> is the behavior of resistance on removal of the single shot photon field of duration  $\approx 6 \text{ ns}$ . In the present case the system recovers its insulating state on removal of the photon field. In PCMO, however, the photoinduced metallic state persists as long as the bias voltage is present. The sample goes back to the insulating state on removal of the bias. If the strength of the CO state in PCMO is weakened through bandwidth control, the photoinduced metallic state survives even on removal of the bias, as seen in the case of  $\text{Pr}_{0.55}(\text{Ca}_{1-Y}\text{Sr}_Y)_{0.45}\text{MnO}_3$  ( $0.2 \leq y \leq 0.4$ ).<sup>11</sup> The absence of a persistent metallic state in these BCMO films after the single-shot photoexposure is an indication of the high stability of the CO-state. This inference is consistent with the results of electric and magnetic field induced changes in charge transport, both of which reveal a robust CO-state. An interesting aspect of photoillumination emerges when the sample is driven to the conducting state by applying voltages more than critical switching field. A typical response of the sample in the field-driven metallic state is shown in Fig. 19. Unlike the previous case, here both the leading and the trailing edges of the conductivity profile follow the shape of the laser pulse. The characteristic recovery time  $\tau$  in this case is only  $\approx 60 \text{ ns}$ . This observation further suggests that the long recovery processes (several microseconds) seen in Fig. 17 and 18 is due to the reappearance of COI domains which had melted under photoillumination. Finally we compare our results of pulsed laser irradiation of BCMO films with the work

on photoillumination of BCMO crystal with a 488 nm CW laser.<sup>6</sup> The irreversible changes seen in the refractive index of those crystals by Smolyaninov *et al.*<sup>6</sup> were realized at a much higher photon flux ( $\approx 10^{24}$  photon/mm<sup>2</sup>). We believe the reversibility seen in our films is due to the lower photon flux used in these experiments. The CO-state in films is also likely to get pinned by growth related strain and defects.

## E. CONCLUSIONS

In conclusion, epitaxial thin films of  $\text{Bi}_{1-x}\text{Ca}_x\text{MnO}_3$  ( $x = 0.6, 0.67, 0.76$ ) were grown on LAO (100) and STO (100) substrates using pulsed laser deposition. The out-of-plane lattice parameter of the films is a sensitive function of the  $T_D$  and  $p\text{O}_2$  and the lattice parameter of the substrate, and plays a key role in setting the temperature scale for charge ordering. Magnetization measurements on  $\text{Bi}_{0.4}\text{Ca}_{0.6}\text{MnO}_3$  grown on LAO under optimal condition reveal a  $T_{CO}$  of  $\approx 275$  K and no signatures of  $T_N$  unlike in bulk samples for which  $T_{CO} \approx 330$  K and  $T_N \approx 125$  K. However,  $\text{Bi}_{0.4}\text{Ca}_{0.6}\text{MnO}_3$  grown on STO exhibits  $T_{CO} \approx 300$  K and  $T_N \approx 120$  K apart from a small ferromagnetic phase below 50 K. This difference can be attributed to the fact that BCMO grown on STO experiences an in-plane tensile strain owing to the difference in their lattice parameters. Electrical transport in the charge-ordered state has signatures of variable range hopping in a three dimensional disordered system, which presumably results from the A site ionic size and positional disorder in the perovskite lattice. I-V measurements on the  $\text{Bi}_{0.4}\text{Ca}_{0.6}\text{MnO}_3$  exhibited hysteretic current switching with a history dependent voltage threshold which appears to be a compound effect of joule heating and permanent changes in the topology of the CO state. Photoresponse measurements using nano second pulses of the third harmonic of Nd-YAG laser were performed on  $\text{Bi}_{0.4}\text{Ca}_{0.6}\text{MnO}_3$  both in its insulating state as well as the electric field induced metallic state. The response was transient with a lifetime of  $\approx 2.4 \mu\text{s}$  and 60 ns for the insulating and metallic states respectively. Unlike the case of some less-than-half-filled CO manganites of intermediate bandwidth where the photoinduced conducting state persists on removal of the photon field, the quick recovery seen here indicates that the CO state is quite robust in these  $\text{Bi}_{0.4}\text{Ca}_{0.6}\text{MnO}_3$  epitaxial films.

## ACKNOWLEDGEMENTS

This research has been supported by a grant from the Indo-French Centre for Promotion

of Advanced Research (IFCPAR) New Delhi, India.

---

\* Electronic address: rcb@iitk.ac.in

- <sup>1</sup> V. A. Bokov, N. A. Grigoryan, and M. F. Bryzhina, *Phys. Status Solidi* **20**, 745 (1967).
- <sup>2</sup> H. Chiba, T. Atou, H. Faqir, M. Kikuchi, Y. Syono, Y. Murakami, and D. Shindo, *Solid State Ionics* **108**, 193 (1998).
- <sup>3</sup> H. Woo, T.A. Tyson, M. Croft, S-W. Cheong, and J.C. Woicik, *Phys. Rev. B* **63**, 134412 (2001).
- <sup>4</sup> H. Chiba, M. Kikuchi, K. Kusaba, Y. Muraoka, and Y. Syono, *Solid State Commun.* **99**, 499 (1996).
- <sup>5</sup> V. Podzorov, B.-G. Kim, V. Kiryukhin, M. E. Gershenson, and S.-W. Cheong, *Phys. Rev. B* **64**, 140406 (2001).
- <sup>6</sup> I.I. Smolyaninov, V.N. Smolyaninova, C.C. Davis, B.-G. Kim, S.-W. Cheong, and R.L. Greene, *Phys. Rev. Lett.* **87**, 127204 (2001).
- <sup>7</sup> Hyungje Woo, Trevor A Tyson, Mark Croft and Sang-Wook Cheong, *J. Phys.: Condens. Matter* **16**, 2689 (2004).
- <sup>8</sup> K. Miyano, T. Tanaka, Y. Tomioka, and Y. Tokura, *Phys. Rev. Lett.* **78**, 4257 (1997).
- <sup>9</sup> T. Tonogai, T. Satoh, K. Miyano, Y. Tomioka, and Y. Tokura, *Phys. Rev. B* **62**, 13903 (2000).
- <sup>10</sup> M. Fiebig, K. Miyano, T Satoh, Y. Tomioka, and Y. Tokura, *Phys. Rev. B* **60**, 7944 (1999).
- <sup>11</sup> N. Takubo, Y.Ogimoto, M. Nakamura, H. Tamaru, M. Izumi, and K. Miyano, *Phys. Rev. Lett.* **95**, 017404 (2005).
- <sup>12</sup> R. Cauro, A. Gilabert, J. P. Contour, R. Lyonnet, M.-G. Medici, J.-C. Grenet, C. Leighton, and Ivan K. Schuller, *Phys. Rev. B* **63**, 174423 (2001).
- <sup>13</sup> H. Huhtinen, R. Laiho, E. Lähderanta, L. S. Vlasenko, M. P. Vlasenko, and V. S. Zakhvalinskii, *Phys. Rev. B* **62**, 11614 (2000).
- <sup>14</sup> H. Oshima, M. Nakamura, and K. Miyano, *Phys. Rev. B* **63**, 075111 (2001).
- <sup>15</sup> J. M. Dai, W. H. Song, J. J. Du, J. N. Wang, and Y. P. Sun, *Phys. Rev. B* **67**, 144405 (2003).
- <sup>16</sup> K. Ogawa, W. Wei, K. Miyano, Y. Tomioka, and Y. Tokura, *Phys. Rev. B* **57**, 15033 (1998).
- <sup>17</sup> H. Katsu, H. Tanaka, and T. Kawai, *Appl. Phys. Lett.* **76**, 3245 (2000).
- <sup>18</sup> M. Fiebig, K. Miyano, Y. Tomioka, and Y. Tokura, *Science*, **280**, 1925 (1998).
- <sup>19</sup> V. N. Smolyaninova, M. Rajeswari, R. Kennedy, M. Overby, S. E. Lofland, L. Z. Chen, and R. L. Greene, *Appl. Phys. Lett.* **86**, 071922 (2005).

- <sup>20</sup> A. J. Millis, T. Darling, and A. Migliori, *J. Appl. Phys.* **83**, 1588 (1998).
- <sup>21</sup> N.-C. Yeh, C.-C. Fu, J. Y. T. Wei, R. P. Vasquez, J. Huynh, S. M. Maurer, G. Beach, and D. A. Beam, *J. Appl. Phys.* **81**, 5499 (1997).
- <sup>22</sup> M. Bibes, S. Valencia, Ll. Balcells, B. Martinez, J. Fontcuberta, M. Wojcik, S. Nadolski, and E. Jedryka, *Phys. Rev. B* **66**, 134416 (2002).
- <sup>23</sup> *Electronic Processes in Non-Crystalline Solids*, 2nd ed. N. F. Mott and E. A. Davies, (Oxford University, New York, 1979).
- <sup>24</sup> V. N. Smolyaninova, Amlan Biswas, X. Zhang, K. H. Kim, Bog-Gi. Kim, S-W. Cheong, and R. L. Greene, *Phys. Rev. B* **62**, R6093 (2000).
- <sup>25</sup> M. B. Salamon, and M. Jaime, *Rev. Mod. Phys.* **73**, 583 (2001).
- <sup>26</sup> Y. Tokura, and Y. Tomioka, *J. Magn. Magn. Mater.* **200**, 1 (1999).
- <sup>27</sup> S. Srivastava, N. K. Pandey, P. Padhan, and R. C. Budhani, *Phys. Rev. B* **62**, 13868 (2000).
- <sup>28</sup> A. Asamitsu, Y. Tomioka, H. Kuwahara, and Y. Tokura, *Nature (London)*, **388**, 50 (1997).
- <sup>29</sup> A. Palanisami, M. B. Weissman, and N. D. Mathur, *Phys. Rev. B* **71**, 094419 (2005).
- <sup>30</sup> C. N. R. Rao, A. R. Raju, V. Ponnambalam, S. Parasar, and N. Kumar, *Phys. Rev. B* **61**, 594 (2000).
- <sup>31</sup> H. Oshima, K. Miyano, Y. Konishi, M. Kawasaki, and Y. Tokura, *Appl. Phys. Lett.* **75**, 1473 (1999).
- <sup>32</sup> *Colossal Magnetoresistance, Charge-ordering and Related Aspects of Manganese Oxides*, C.N.R. Rao and B. Raveau (Eds.), (World Scientific, Singapore, 1998).
- <sup>33</sup> *Colossal Magnetoresistive Oxides*, Tokura Y. (Ed.), (Gordon and Breach, London, 2000).
- <sup>34</sup> J. M. D. Coey, M. Viret, and S. von Molnar, *Adv. Phys.* **48**, 167 (1999).

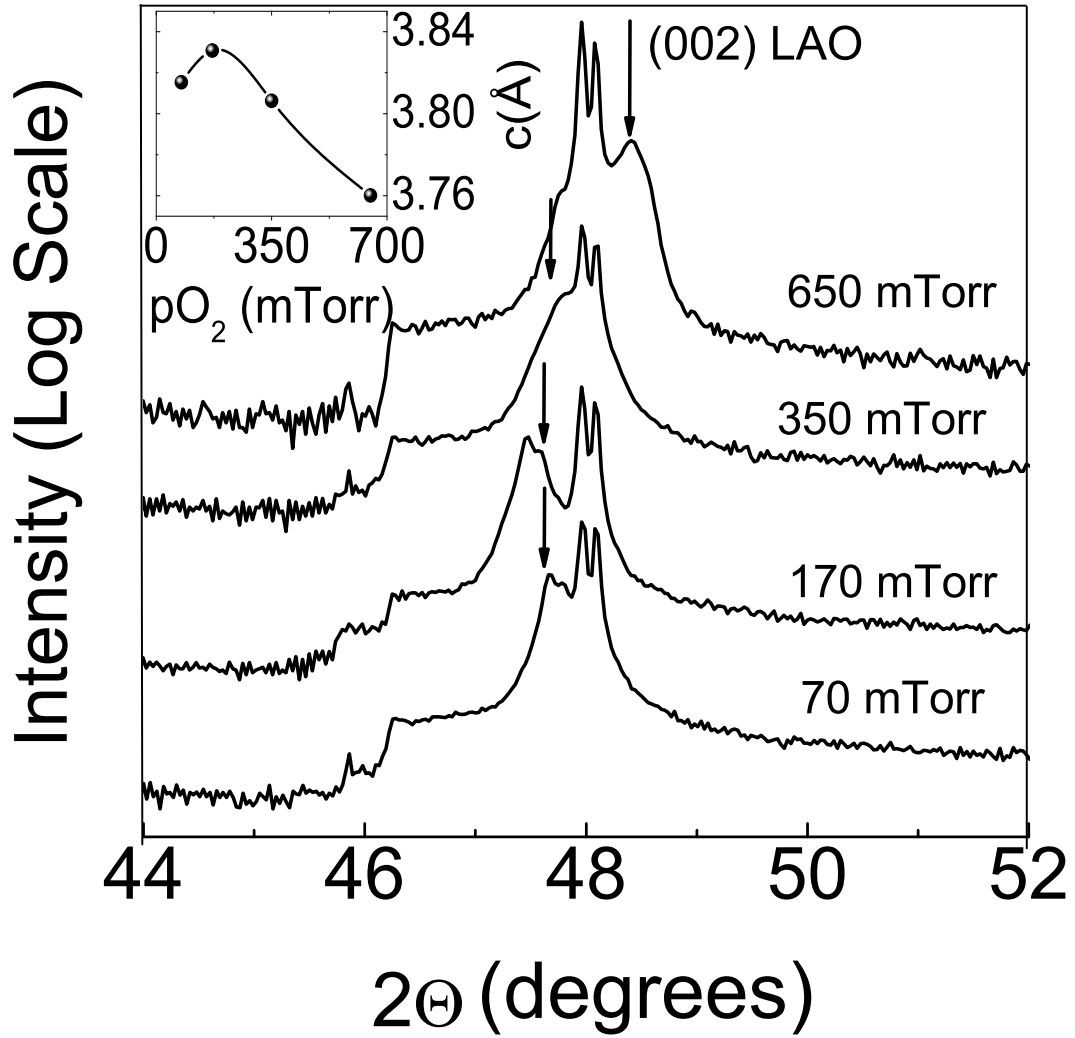


FIG. 1: X-ray diffraction pattern of Bi<sub>1-x</sub>Ca<sub>x</sub>MnO<sub>3</sub> thin films on LAO with x = 0.6 grown at 750 °C under different oxygen partial pressure. The inset shows the variation of the out-of-plane lattice parameter (*c*) with pO<sub>2</sub>. The diffraction peak of the film is marked by arrow.



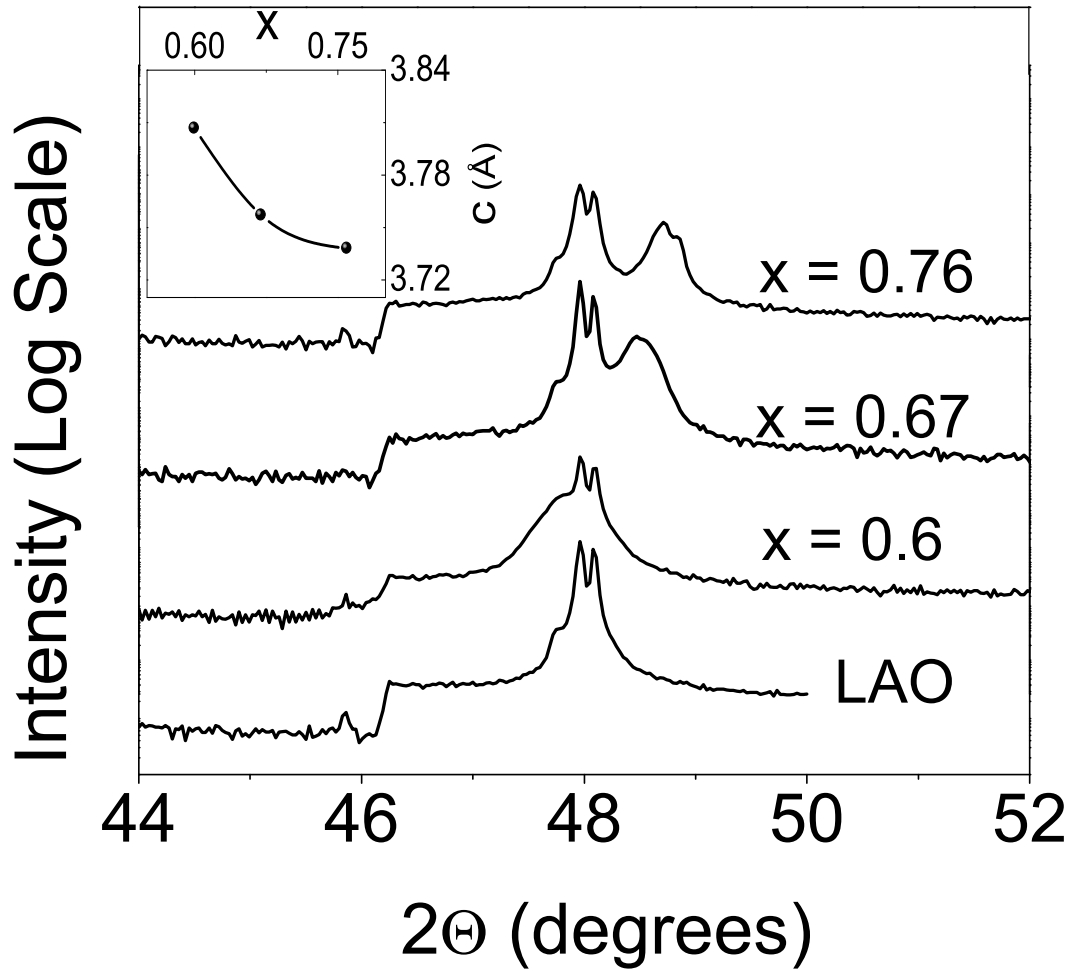


FIG. 2: X-ray diffraction pattern of Bi<sub>1-x</sub>Ca<sub>x</sub>MnO<sub>3</sub> thin films on LAO for different x grown at 750 °C and oxygen partial pressure of 350 mTorr. The inset shows the variation of the out-of-plane lattice parameter with x.

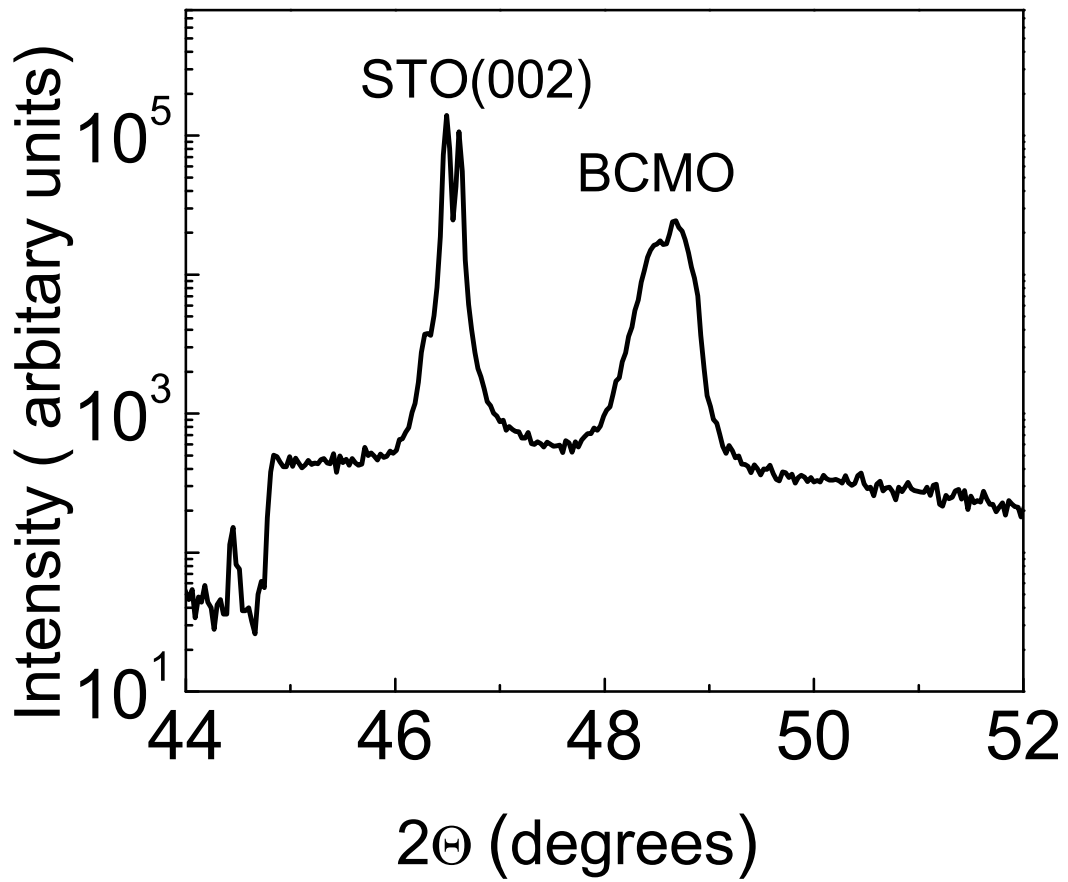


FIG. 3: X-ray diffraction pattern of  $\text{Bi}_{1-x}\text{Ca}_x\text{MnO}_3$  thin films on STO with  $x = 0.6$  grown at oxygen partial pressure of 350 mTorr and  $T_D \approx 750^\circ\text{C}$ .

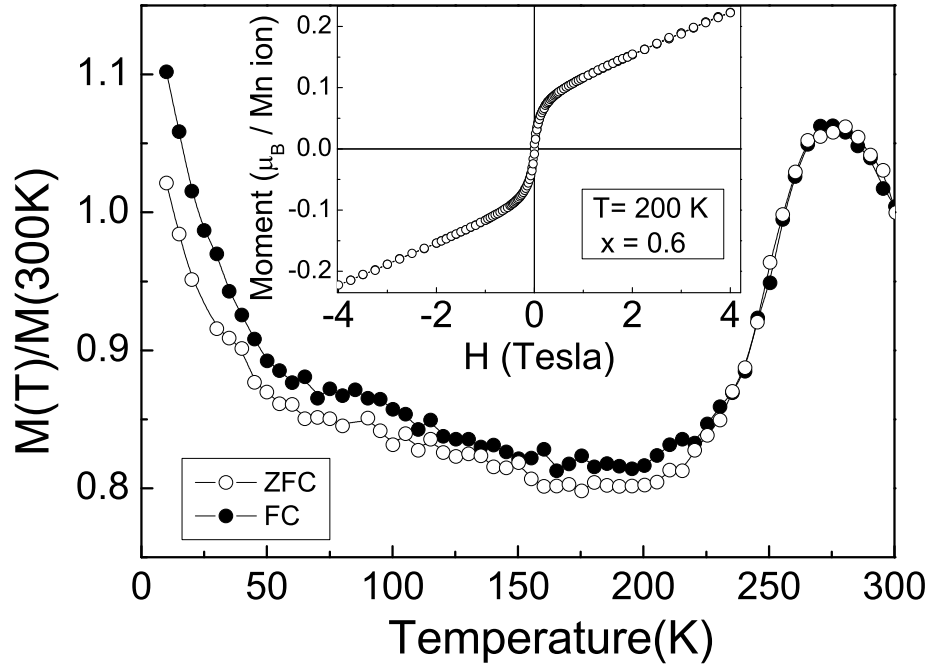


FIG. 4: Field-cooled and Zero-field-cooled magnetization vs temperature plots for  $\text{Bi}_{0.4}\text{Ca}_{0.6}\text{MnO}_3$  film on LAO grown at  $750^\circ\text{C}$  and 350 mTorr. The measurements were performed in an in-plane field of 0.5 T. The peak at  $\approx 275$  K corresponds to  $T_{CO}$ . Inset shows the behavior of magnetization as a function of field at 200 K.

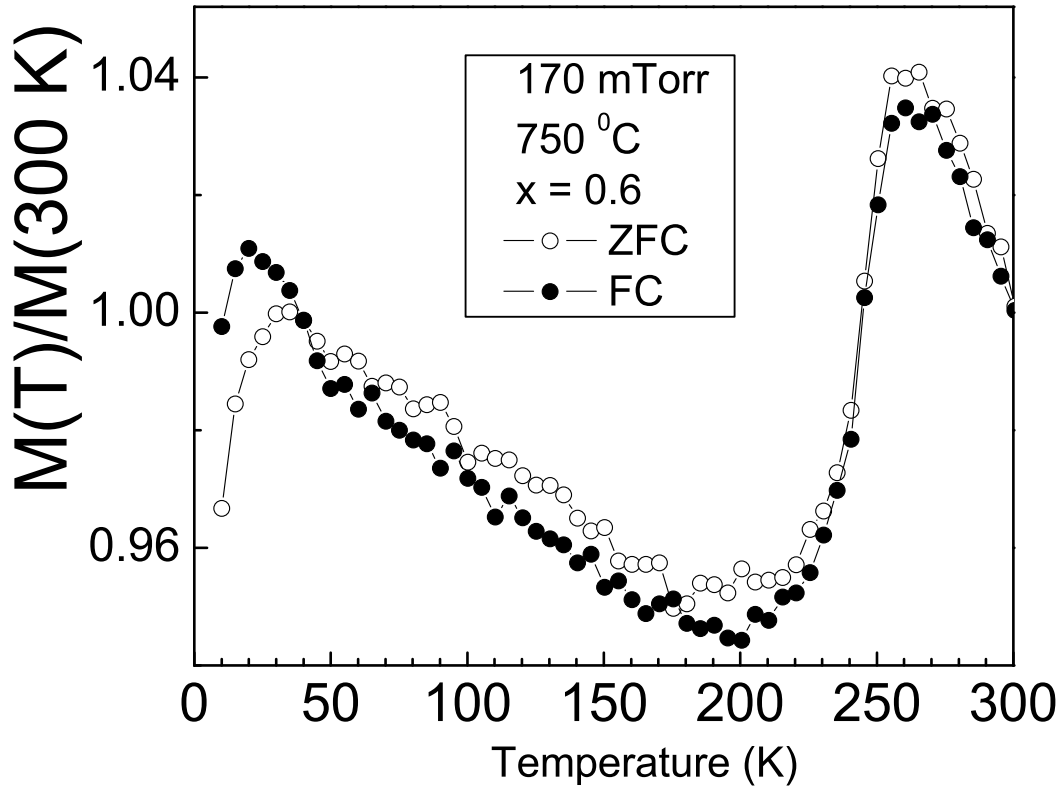


FIG. 5: Field-cooled and Zero-field-cooled magnetization vs temperature plots for  $\text{Bi}_{0.4}\text{Ca}_{0.6}\text{MnO}_3$  film on LAO grown at  $750^\circ\text{C}$  and 170 mTorr. The measurements were performed in an in-plane field of 0.5 T. The peak at  $\approx 260$  K corresponds to  $T_{CO}$ .

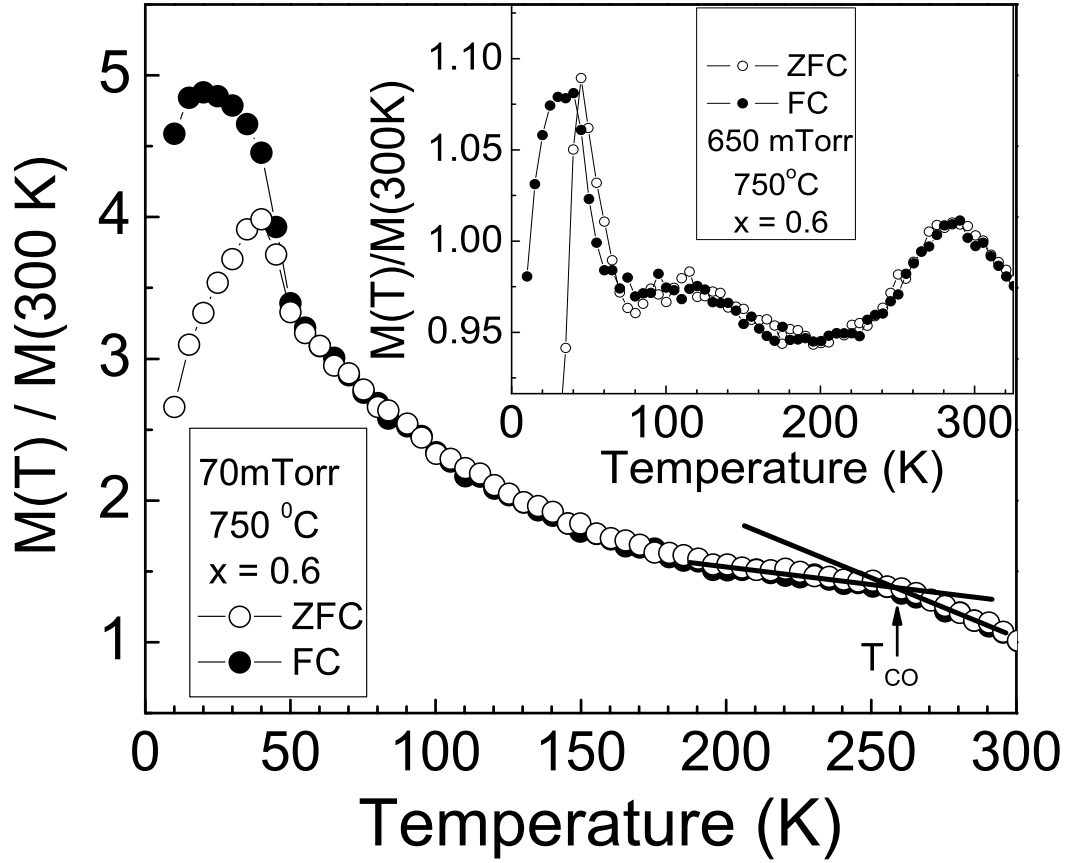


FIG. 6: Field-cooled and Zero-field-cooled magnetization vs temperature plots for  $\text{Bi}_{0.4}\text{Ca}_{0.6}\text{MnO}_3$  film on LAO grown at  $750\text{ }^\circ\text{C}$  and  $70\text{ mTorr}$ . The measurements were performed in an in-plane field of  $0.5\text{ T}$ . There is no signature of  $T_{CO}$  in the data. The inset shows the magnetization measurement of the  $x = 0.6$  sample deposited at  $750\text{ }^\circ\text{C}$  and  $650\text{ mTorr}$  in an in-plane field of  $0.5\text{ T}$ . The peak at  $\approx 285\text{ K}$  and  $110\text{ K}$  corresponds to  $T_{CO}$  and  $T_N$  respectively.

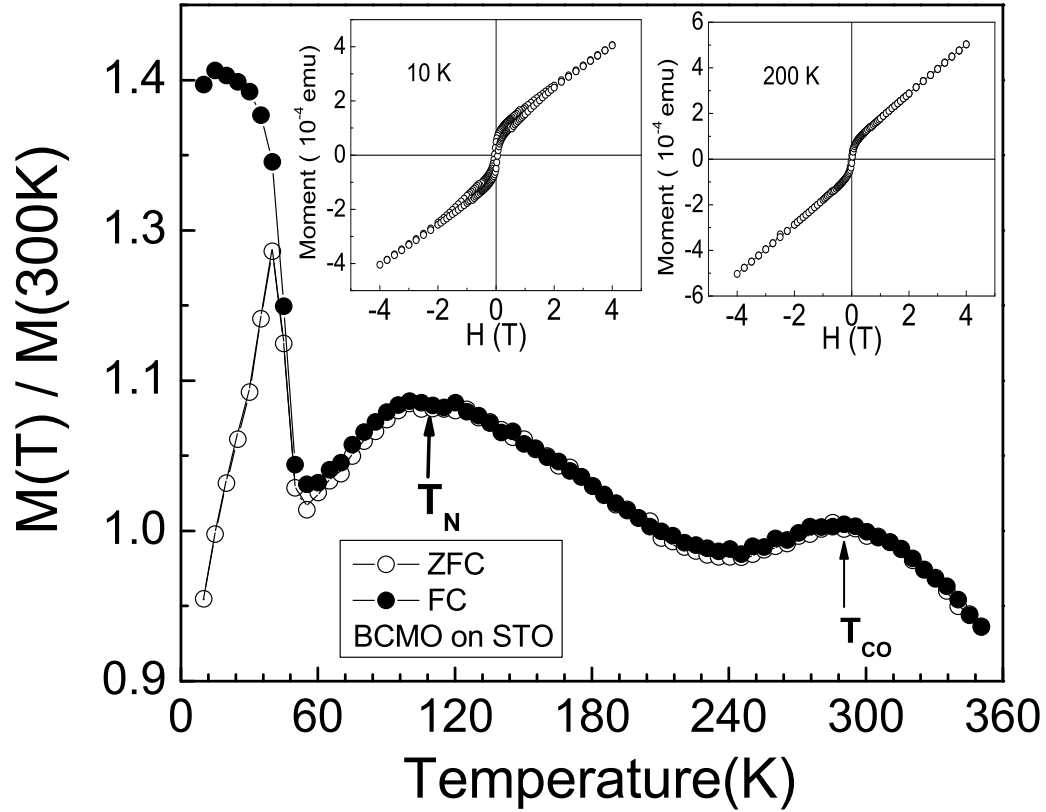


FIG. 7: Field-cooled and Zero-field-cooled magnetization vs temperature plots for a  $\text{Bi}_{0.4}\text{Ca}_{0.6}\text{MnO}_3$  film deposited on STO at  $750^\circ\text{C}$  and 350 mTorr of  $\text{pO}_2$ . The applied field of 0.5 T was in the plane of the film. The peak at  $\approx 300$  K and  $\approx 125$  K corresponds to  $T_{CO}$  and  $T_N$  respectively. The inset shows M-H data at 10 K and 200 K.

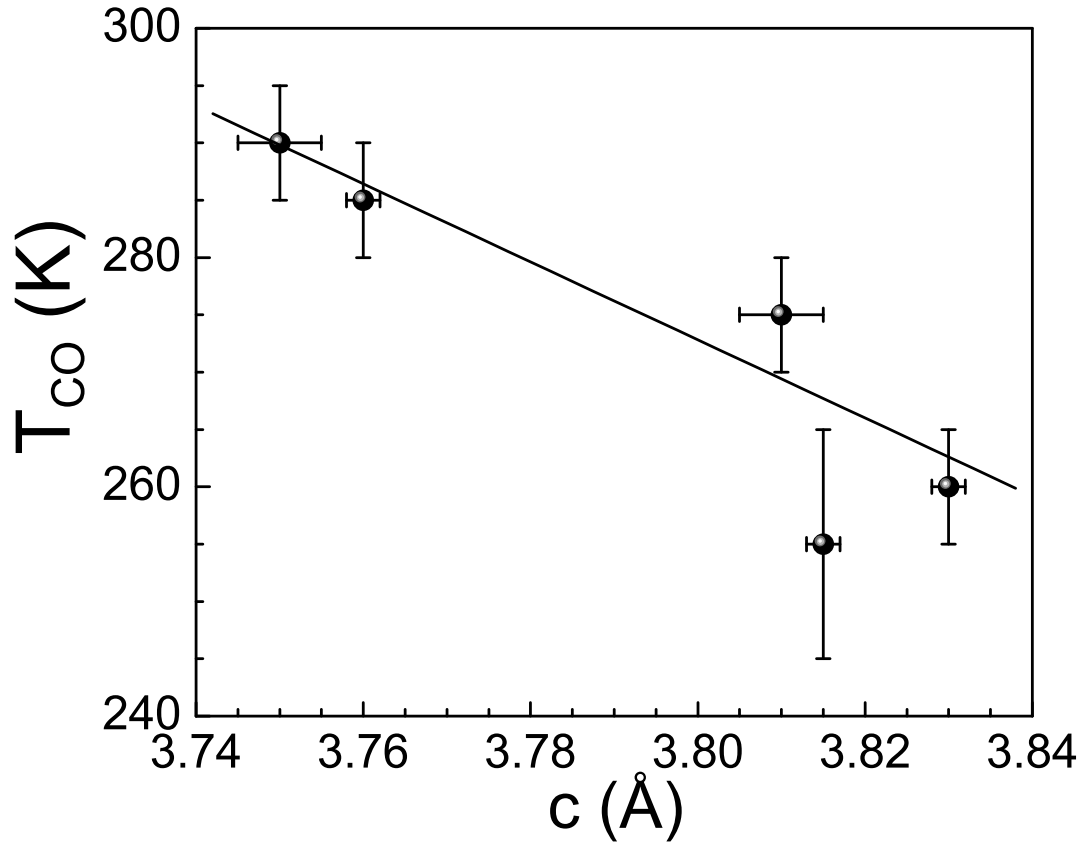


FIG. 8: The variation of  $T_{CO}$  with out of plane lattice parameter ( $c$ ) for BCMO with  $x = 0.6$  and deposited at  $750^{\circ}\text{C}$ .

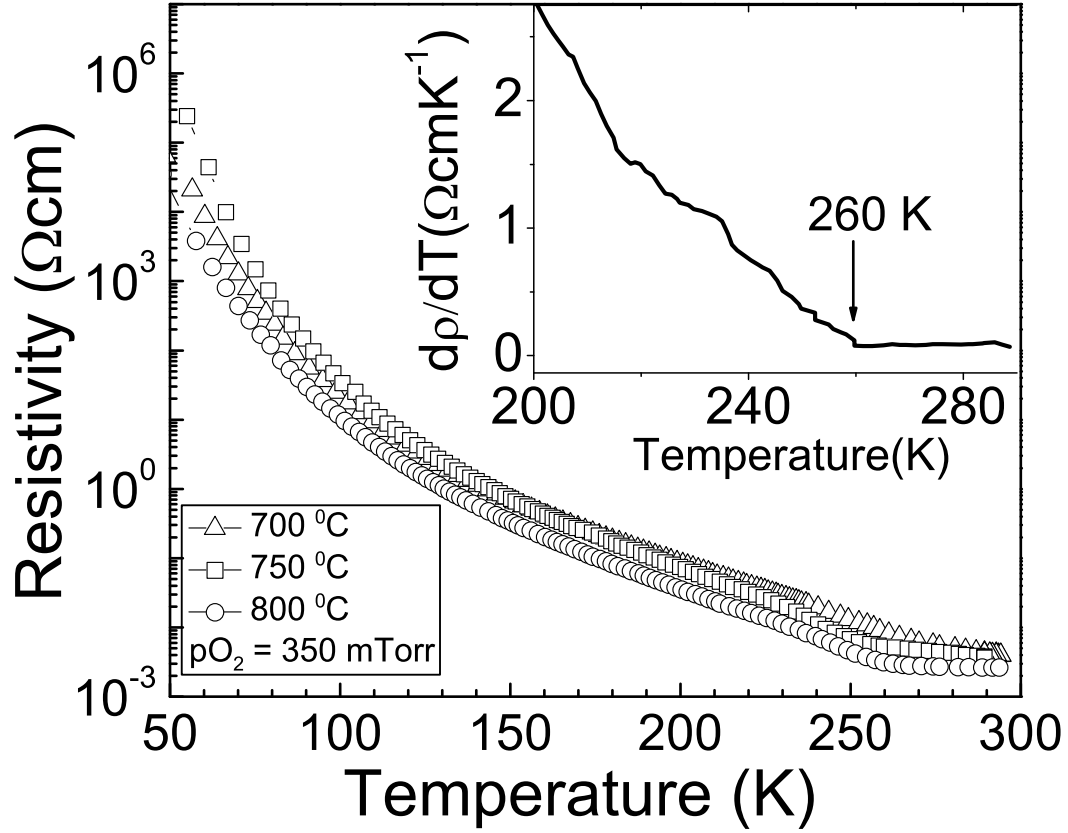


FIG. 9: Electrical resistivity of  $\text{Bi}_{0.4}\text{Ca}_{0.6}\text{MnO}_3$  thin films deposited on LAO at a fixed  $p\text{O}_2$  (350 mTorr) but at different temperatures ( $T_D$ ) plotted as a function of temperature. A pronounced step at  $\approx 260$  K is observed for the sample with  $T_D$  of  $\approx 750$  °C. The inset shows the differential resistivity as a function of temperature for the same sample.



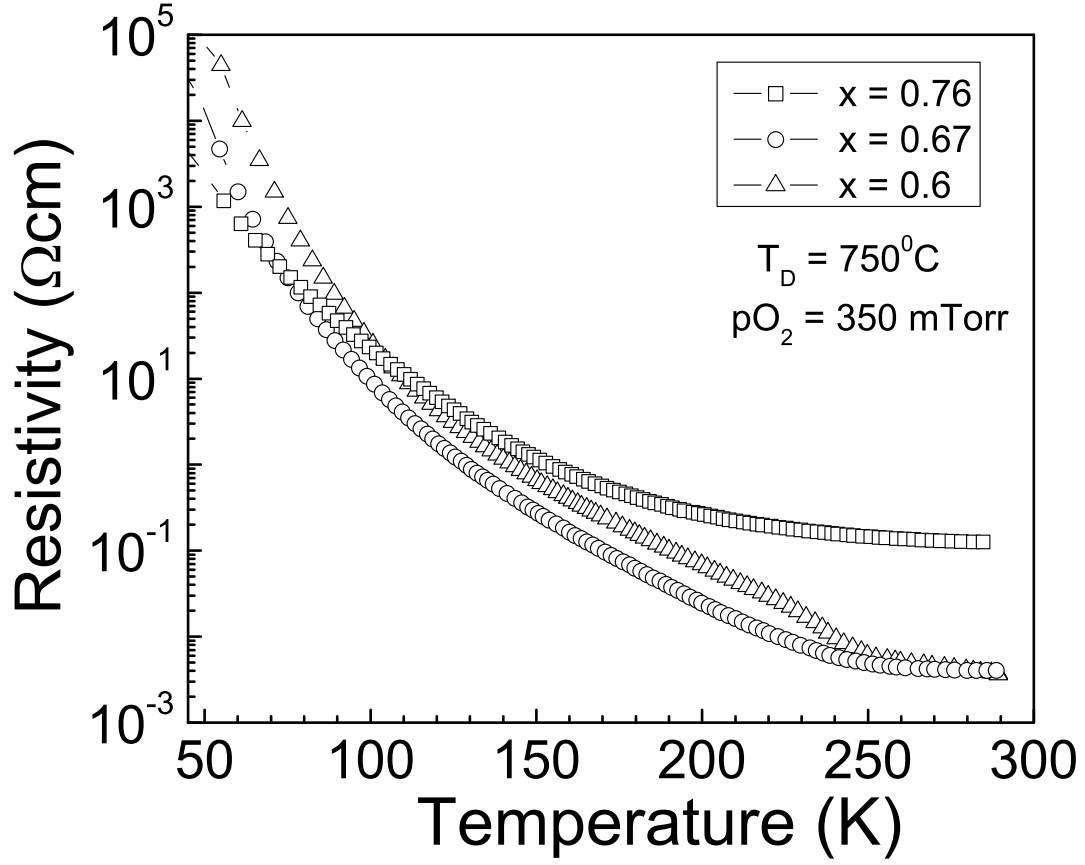


FIG. 10: Electrical resistivity of  $\text{Bi}_{1-x}\text{Ca}_x\text{MnO}_3$  ( $x = 0.6, 0.67, 0.76$ ) thin films deposited on LAO at  $T_D \approx 750^\circ\text{C}$  and  $p\text{O}_2$  of 350 mTorr plotted as a function of temperature. A pronounced step at  $\approx 260$  K is observed for the sample with  $x = 0.6$ .

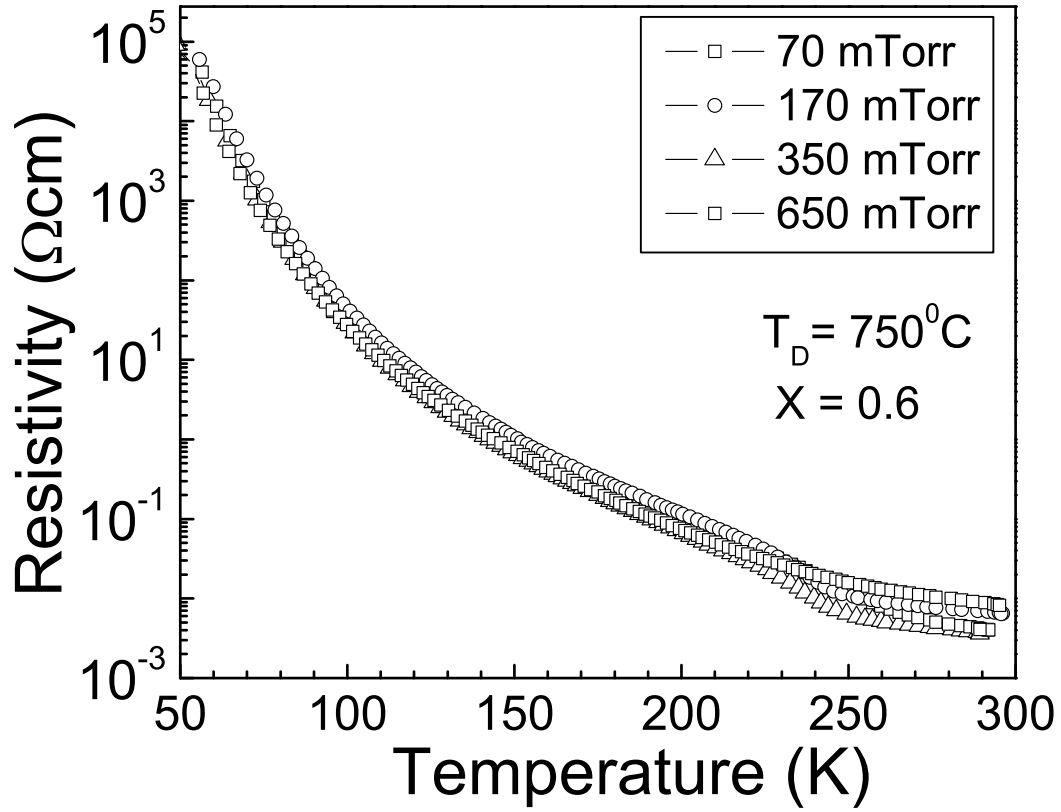


FIG. 11: Electrical resistivity of  $\text{Bi}_{0.4}\text{Ca}_{0.6}\text{MnO}_3$  thin films deposited on LAO at  $T_D \approx 750^\circ\text{C}$  but at different oxygen partial pressure ( $p\text{O}_2$ ) plotted as a function of temperature. A pronounced step at  $\approx 260$  K is observed for the sample deposited at 350 mTorr.

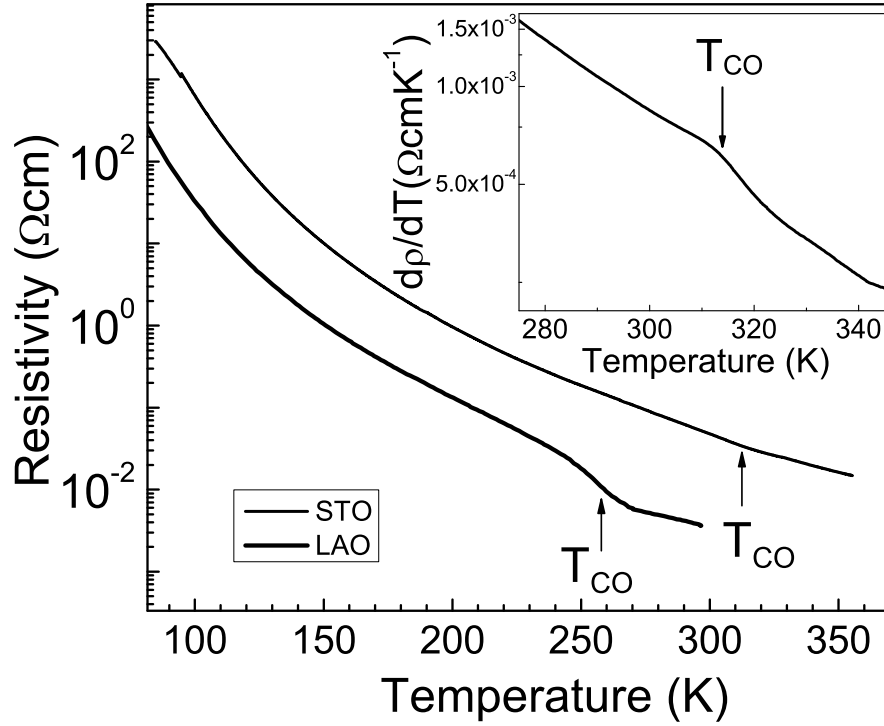


FIG. 12: Electrical resistivity of  $\text{Bi}_{0.4}\text{Ca}_{0.6}\text{MnO}_3$  thin films deposited on STO and LAO at  $750^\circ\text{C}$  and  $p\text{O}_2$  of 350 mTorr plotted as a function of temperature. The inset shows the differential resistivity as a function of temperature for the sample on STO. The kink at  $\approx 310$  K corresponds to  $T_{CO}$ .

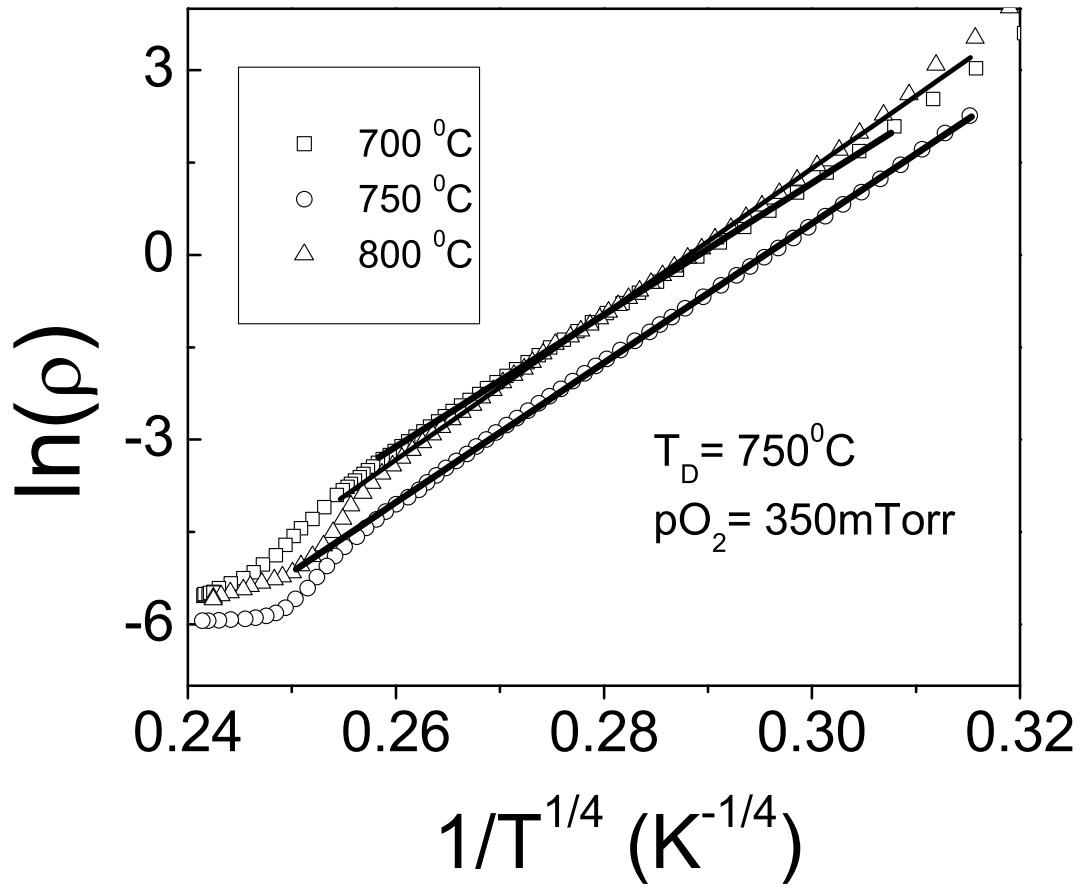


FIG. 13:  $\ln(\rho(T))$  vs  $T^{-1/4}$  plots for the sample with  $x = 0.6$  grown at fixed  $p\text{O}_2$  (350 mTorr) but different deposition temperature of 700 °C, 750 °C and 800 °C. The solid lines show fitting to the variable range hopping formula  $\rho(T) = \rho_0 \exp [T_0/T]^{1/4}$ .

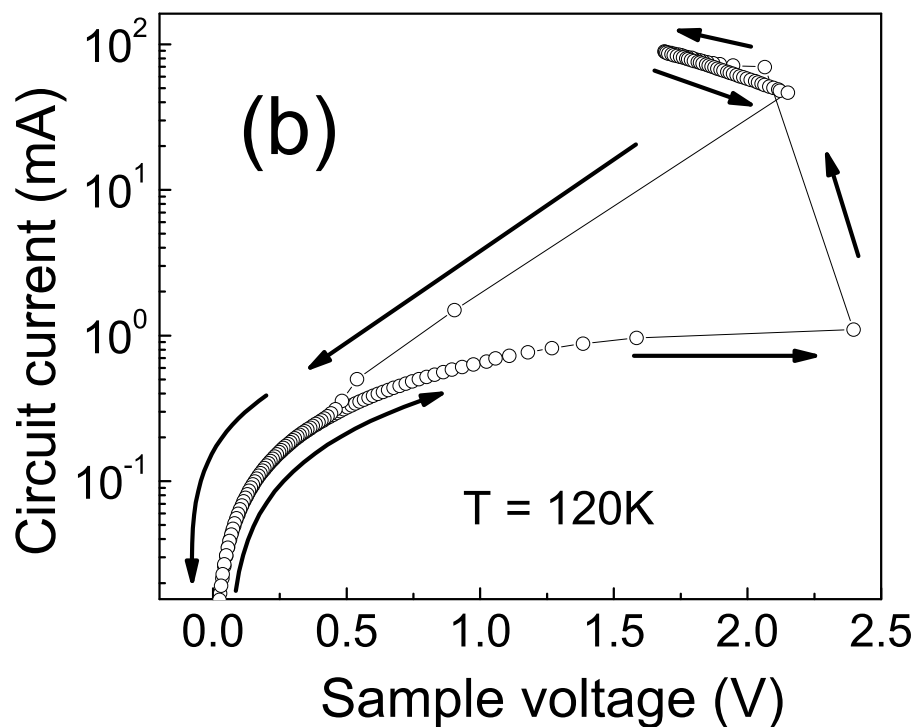
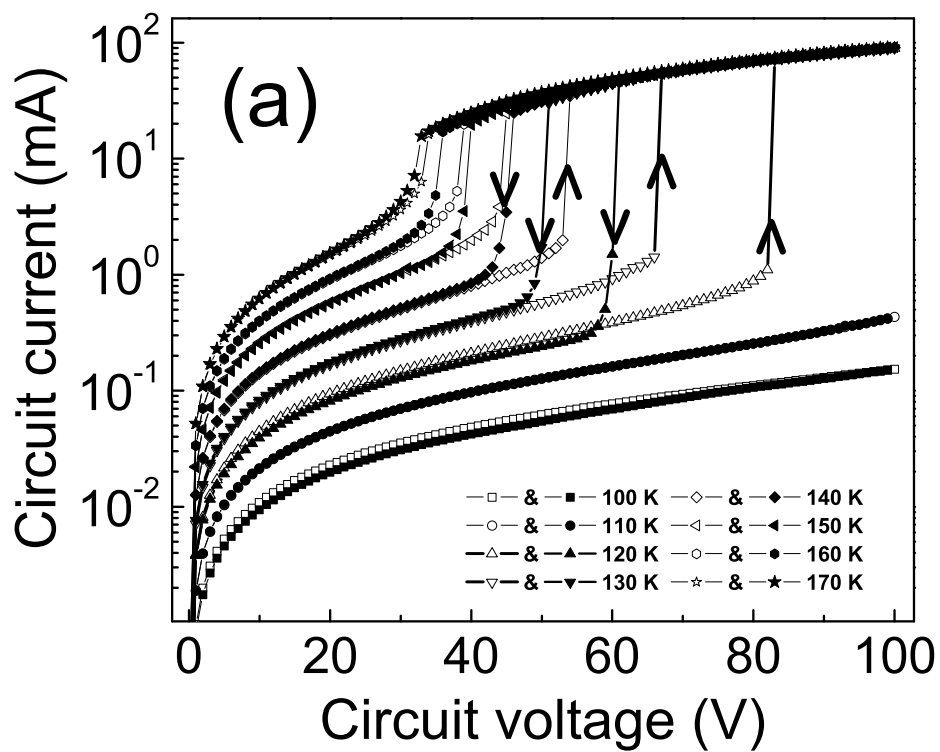


FIG. 14: (a) I-V characteristics of the circuit comprising of the BCMO film ( $x = 0.6$ ) deposited at  $750^\circ\text{C}$  and a  $1\text{ k}\Omega$  resistor in series. The measurements have been done at different temperatures. The open and filled symbols correspond to the increasing and decreasing branch of the voltage

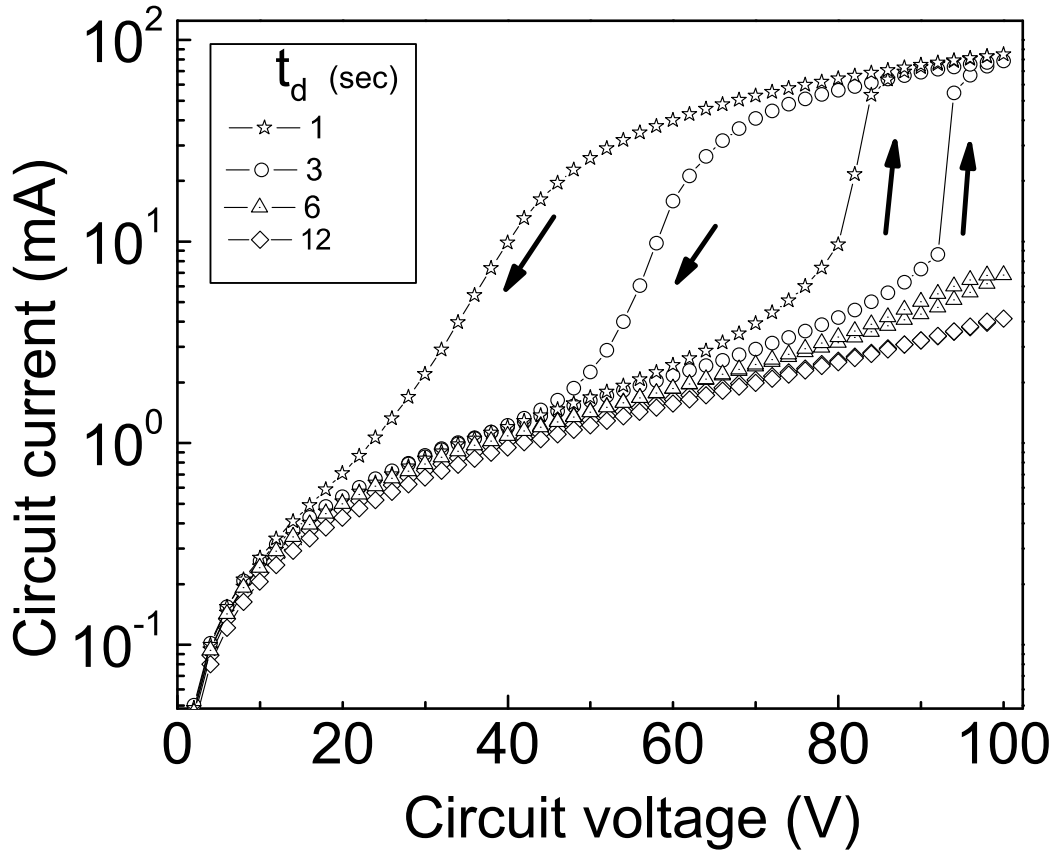


FIG. 15: The variation of circuit current ( $I$ ) as a function of applied voltage ( $V$ ) at 120 K. The measurements were done by increasing the voltage in a stepped manner. The parameter  $t_d$  is the time during which the voltage pulse was off. The increasing and the decreasing branches of the I-V are marked.

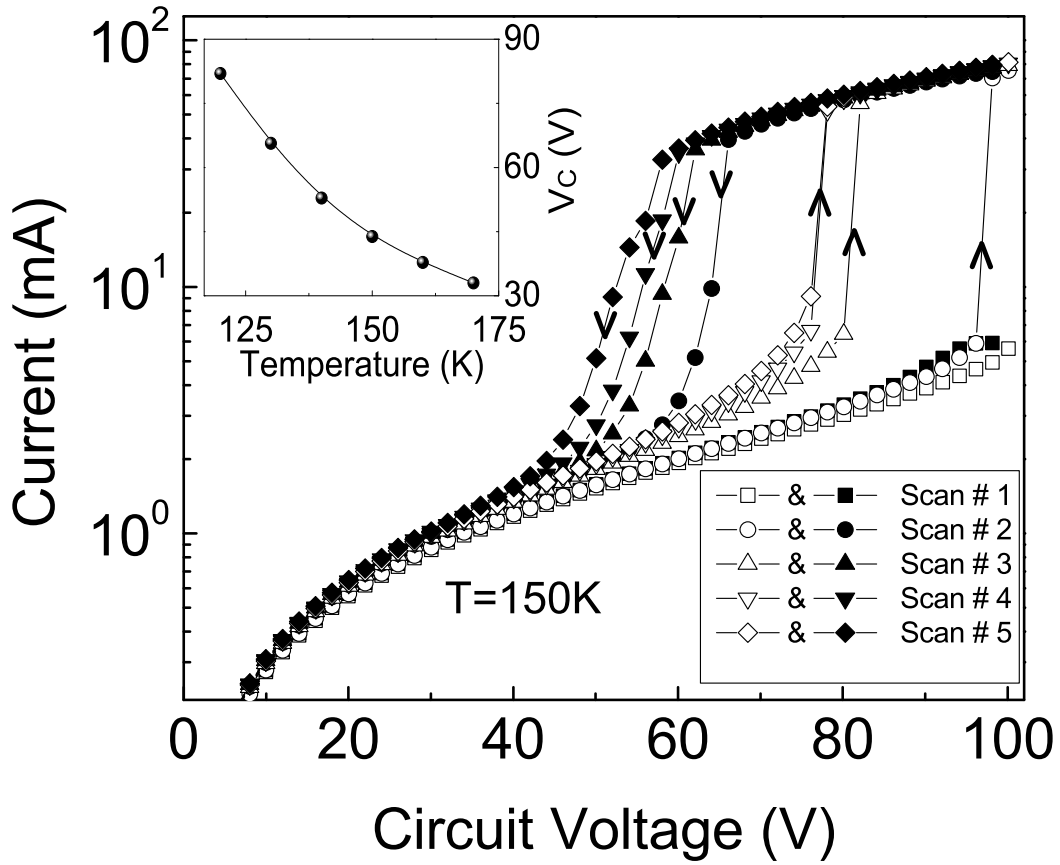


FIG. 16: The variation of circuit current ( $I$ ) as a function of applied ( $V$ ) at 150 K for successive scans. The open symbols correspond to ramping the voltage to higher values and the closed one corresponds to the reverse ramping. The inset shows the variation of the critical applied circuit voltage  $V_C^*$  (at which the sample goes to a conducting state) as a function of temperature.

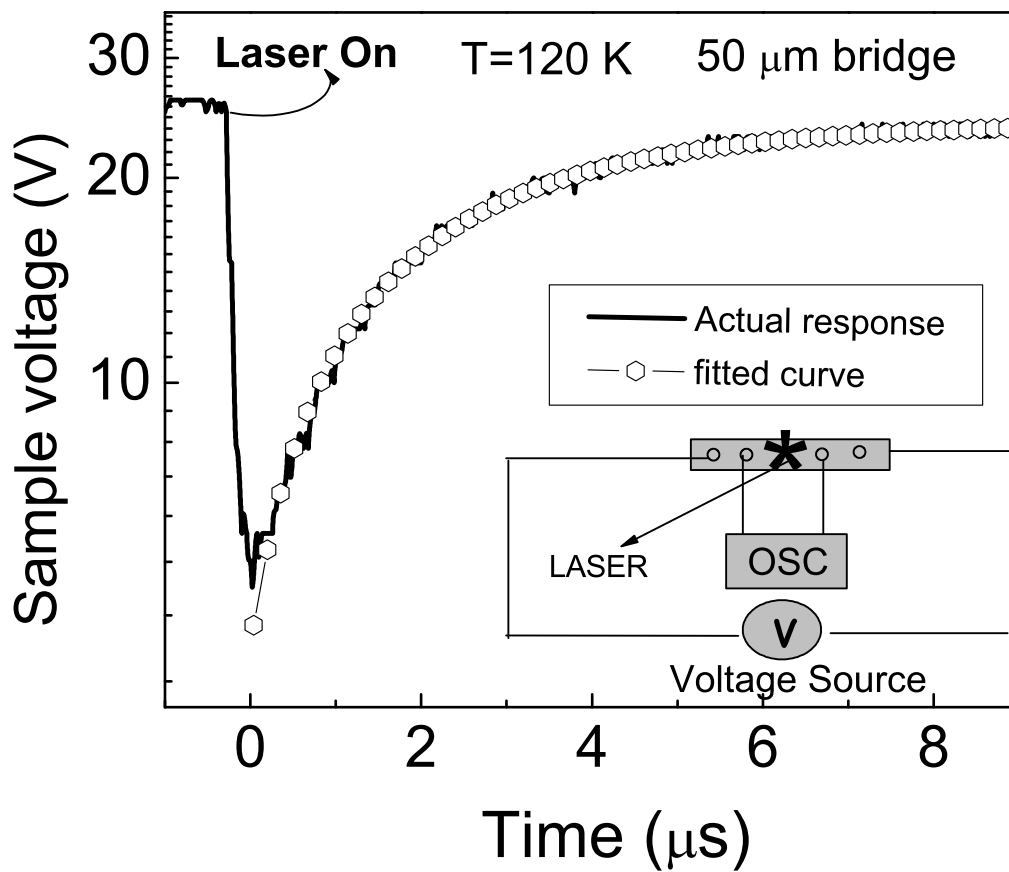


FIG. 17: The variation of the sample voltage in real time as a result of photoillumination at 120 K where the sample is initially in the charge ordered insulating state. The sample regains its original insulating state in about  $2.4 \mu\text{s}$  after switching off the 6 ns photon pulse. The basic circuit diagram is shown in the bottom right corner.



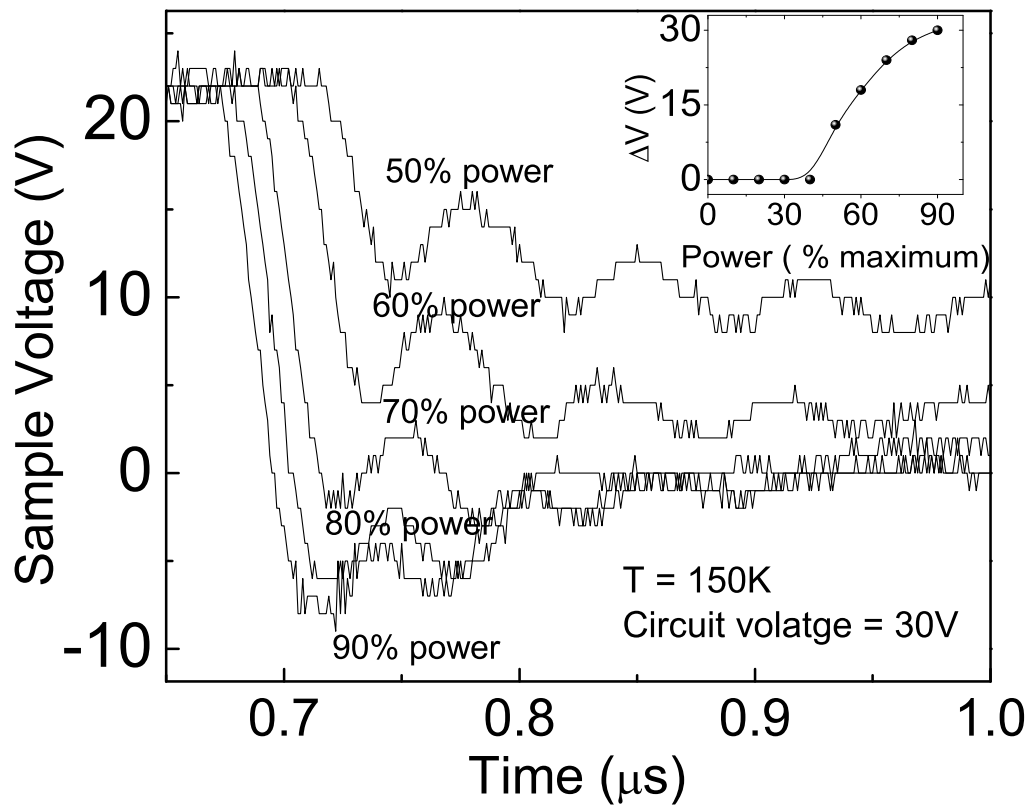


FIG. 18: The variation of the sample voltage in real time for different intensity of the 6 ns laser pulse. The sample held at 150 K with applied bias voltage less than the critical voltage for current switching. The inset shows the maximum drop in voltage ( $\Delta V$ ) that takes place across the sample on photoexposure as a function of laser power.

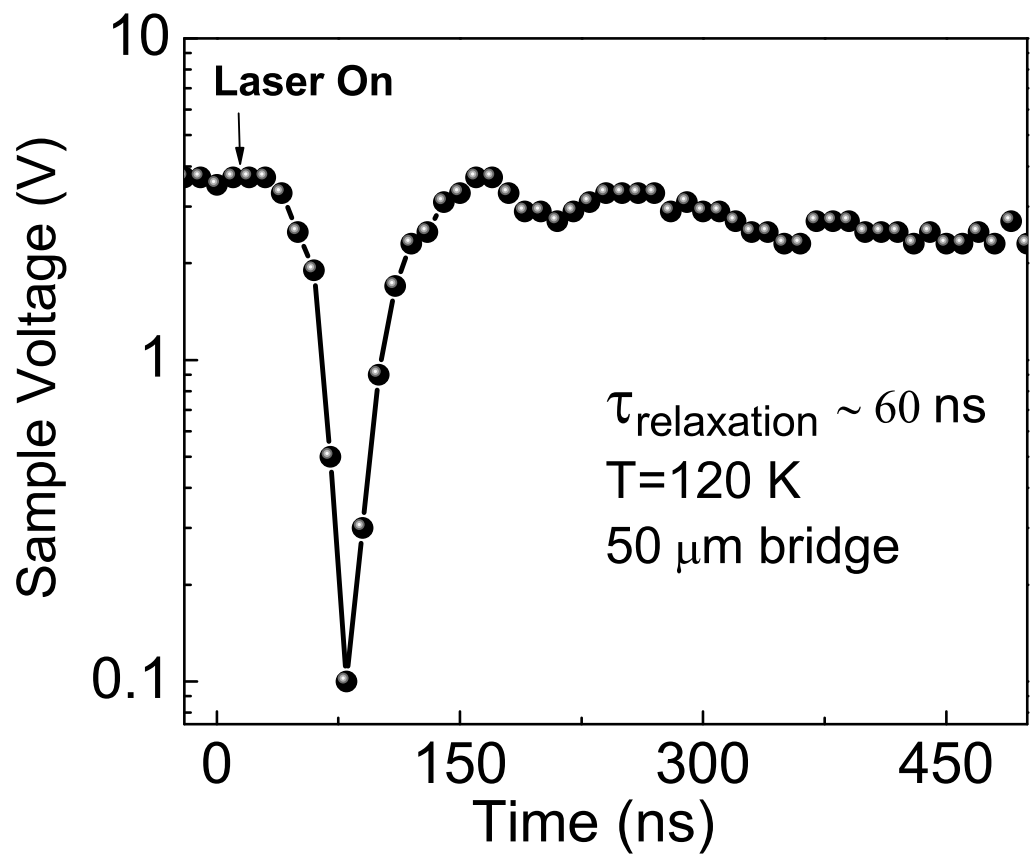


FIG. 19: Real time variation of the sample voltage as a result of photoillumination at 120 K where the sample is initially driven to the metallic state by applying an electric field. In this case the sample relaxes to its initial state in about 60 ns. The solid lines are a guide to the eye.